All-Aramid Composites by Partial Fiber Dissolution

Jian Min Zhang,[†] Zeinab Mousavi,[†] Nattakan Soykeabkaew,[†,‡] Paul Smith,[§] Takashi Nishino,[∥] and Ton Peijs*[,†,⊥]

School of Engineering and Materials Science, Centre for Materials Research, Queen Mary University of London, Mile End Road, E1 4NS London, United Kingdom, School of Science, Mae Fah Luang University, Chiang Rai 57100, Thailand, Department of Materials, ETH Zürich, Wolfgang-Pauli-Strasse 10, 8093 Zürich, Switzerland, Graduate School of Engineering, Department of Chemical Science & Engineering, Kobe University, Rokko, Nada, Kobe 657-8501, Japan, and Eindhoven Polymer Laboratories, Eindhoven University of Technology, 5600MB Eindhoven, The Netherlands

ABSTRACT The area of self-reinforced polymer composites is one of the fastest growing areas in engineering polymers, but until now these materials have been mainly developed on the basis of thermoplastic fibers of moderate performance. In this work, we report on a new type of self-reinforced composites based on high-performance aramid fibers to produce an "all-aramid" composite by applying a surface-dissolution method to fuse poly(*p*-phenylene terephthalamide) (PPTA) fibers together. After immersion in concentrated (95%) sulphuric acid (H_2SO_4) for a selected period of time, partially dissolved fiber surfaces were converted into a PPTA interphase or matrix phase. Following extraction of H_2SO_4 and drying, a consolidated all-aramid composite was formed. The structure, mechanical- and thermal properties of these single-polymer composites were investigated. Optimum processing conditions resulted in unidirectional composites of high reinforcement content (~75 vol %) and good interfacial bonding. The all-aramid composites featured a Young's modulus of ~65 GPa at room temperature, and a tensile strength of 1.4 GPa, which are comparable with or exceed the corresponding values of conventional aramid/epoxy composites. However, since fiber, matrix and interphase in all-aramid composites are based on the same high-temperature resistant PPTA polymer, a high modulus of ~50 GPa was maintained up to 250 °C, demonstrating the potential of these materials for high-temperature applications.

KEYWORDS: aramid fiber • self-reinforced composite • surface dissolution process • high temperature • mechanical properties

INTRODUCTION

Advanced composite materials based on high-performance fibers like aramid or carbon feature excellent mechanical and physical properties and are used in a wide range of applications. In recent years, a new class of "all-polymer composites" or "self-reinforced composites", which are based on similar or identical materials for both matrix and reinforcement, have generated considerable interest because of their advantages in terms of processing and recyclability. Also in terms of interfacial compatibility, these materials have shown beneficial characteristics as both fiber and matrix are of the same chemical origin, unlike traditional fiber reinforced plastics. Numerous studies have been carried out on the preparation and characterization of all-polymer composites based on polyolefins and other polymers, e.g., polyethylene (PE) (1−6), polypropylene (PP) (7−16), poly(ethylene terephthalate) (PET) (17, 18), and liquid-crystalline copolyesters (19). These composites were prepared by a number of techniques which include: film stacking (1, 2, 18), powder impregnation (5), solution impregnation (3), hot-compaction (4, 6−8, 17, 19, 20), and co-extrusion (9−16). Especially the latter two approaches have been fairly successful and have resulted in commercial products. For instance, Curv from Propex Fabrics Inc. is based on a hot-compaction method initially developed at the University of Leeds (4, 20). The process involves the selective melting of polymer fiber skins by carefully controlling the processing temperature and subsequently fusing them together in a compaction process, rather than impregnating fibers with matrix resin as in traditional composite processing. Upon cooling, the molten fiber material recrystallizes into a matrix phase that binds the remaining fibers together, essentially creating a single-polymer composite (4, 20). Furthermore, PURE from Lankhorst Pure Composites BV and Tegris from its licensee Milliken are based on co-extrusion technologies where polypropylene tapes with a thin layer of a lower-melting copolymer are created and drawn into high-strength tapes (9−16). By heating these tapes to a temperature above the melting temperature of the copolymer skins but below that of the oriented cores, we can consolidate these tapes into composite structures with excellent mechanical properties and recyclability (9−16).

Recently, an elegant, complementary surface-dissolution method was developed to prepare all-cellulose composites (21−25). This concept is similar to the surface melting or

* Corresponding author. Tel.: 0044(0) 207 882 8865. E-mail: t.peijs@qmul.ac.uk.
Received for review December 11, 2009 and accepted February 19, 2010
[†] Queen Mary University of London.
[‡] Mae Fah Luang University.
[§] ETH Zürich.
[∥] Kobe University.
[⊥] Eindhoven University of Technology.
DOI: 10.1021/am900859c

hot-compaction method, but based on partial dissolution of the fiber skins rather than melting. Cellulose is well-known not to melt, as it features thermal degradation at temperatures prior to melting. Therefore, solution-based processes were employed to generate all-cellulose composites. In this technique, the matrix phase is formed through selectively dissolving the surface of cellulose fibers in lithium chloride/*N*,*N*-dimethylacetamide (LiCl/DMAc) and, subsequently, consolidating them in a nonsolvent to fuse the fibers together. This surface dissolution method was shown to lead to good interfacial adhesion. The process was applied to a wide range of cellulose materials including filter paper (21), lignocellulose ramie fibers (23), bacterial cellulose (24), and regenerated cellulose (Lyocell and Bocell, a lab-scale cellulose fiber spun from an anisotropic phosphoric acid solution) (25). All these studies demonstrated that composites of high fiber content could be produced and that the mechanical properties of the cellulose fibers could be retained in the composites to a remarkably large extent.

Poly(*p*-phenylene terephthalamide) (PPTA or PPD-T in some literature) or aramid fibers (e.g., Kevlar and Twaron) are among the more important high-performance fibers, with applications in tires, hoses, ballistic and heat protection products, engineering plastics, and composites (26, 27). They combine good mechanical, physical, and chemical properties with a low density (1.44 g/cm^3), and possess high tensile strength (2.3−3.4 GPa), tensile modulus (55−143 GPa), energy absorption combined with low (or negative) coefficient of thermal expansion and relatively good chemical resistance. In addition, these materials are self-extinguishing and have a decomposition temperature exceeding 500 °C (26).

Two main routes exist for the preparation of high-performance polymer fibers. These routes are distinctly different with one being based on flexible macromolecules whereas the other route is based on rigid rod macromolecules. In the case of flexible chain polymers, such as polyethylene in the case of Dyneema and Spectra, solid-state drawing is used to obtain the necessary level of chain extension needed to exploit the intrinsic properties of the polymer chain (28−30). In the case of rigid rod polymers, chain extension is already build in by the chemist and alignment in the extended chain configuration is achieved during fiber spinning, coagulation and heat setting (26, 27, 31, 32). A key factor in the preparation of high strength polymer fibers based on rigid rod polymers is the formation of lyotropic solutions. Kwolek (33) synthesized aromatic polyamides which contained para-oriented cyclic units (*p*-aramids) and observed for the first time these liquid crystalline solutions. These aromatic polyamides were insoluble in conventional media but soluble in strong acids such as sulphuric acid. Rigid rod molecules such as PPTA behave like conventional polymers in dilute solutions where the polymer molecules are randomly oriented and separated beyond the effective range of their intermolecular forces. At higher concentrations, rigid rod molecules will aggregate to form liquid crystalline ordered domains, with the number of ordered domains increasing with solution concentration. PPTA in sulphuric acid forms lyotropic solutions provided that (i) the polymer molecular weight is above a certain limit, (ii) the strength of the sulphuric acid is close to 100%, (iii) the polymer concentration is above a certain limit but below a further, higher limit, and (iv) the temperature is within a specific range (26, 27, 31, 32). Using a dry-jet (air-gap) wet spinning process these anisotropic solutions can be spun into high-tenacity, high-modulus fibers (34). During fiber spinning, the liquid crystal domains in the anisotropic polymer solution will readily undergo orientation under the influence of elongational flow, leading to highly oriented, highly crystalline structures. Kevlar fiber was the first *p*-aramid fiber commercialized by DuPont in the early 1970s. Twaron is another PPTA fiber, originally manufactured by Akzo Nobel and now by Teijin. The concept to obtain high performance fibers from rigid rod polymers has been extensively widened to poly(*p*-phenylene benzobisthiazole) (PBZT) (35, 36), poly(*p*-phenylene beozobisoxazole) (PBO) (37, 38), and poly{diimidazo pyridinylene (dihydroxy) phenylene} (PIPD or "M5") (39, 40).

Traditionally, these high-performance fibers are impregnated with polymer resins to create advanced composite materials. In this study, the aforementioned surface-dissolution method is used to prepare all-aramid composites, where both fiber and matrix are based on PPTA. This yields unique high-temperature-resistant materials with excellent mechanical properties compared to traditional aramid-fiber-reinforced plastics such as aramid/epoxy or other all-polymer composites, which are mainly based on thermoplastic fibers of moderate performance and temperature resistance such as PP and PET.

EXPERIMENTAL SECTION

Materials. Aramid yarn used in this study was Twaron 1000 (standard modulus, dtex = 1735, 1000 filaments per yarn) kindly provided by Teijin Aramid, The Netherlands. The diameter of aramid fibers was measured using scanning electron microscopy. Cross-sectional areas were calculated assuming a circular fiber cross-section.

Sample Preparation. Unidirectional composites were prepared by first aligning the fibers through winding them on a glass frame (Figure 1A). The aligned fibers were constrained to prevent shrinkage and distortion. The assembly of the glass frame comprising the fibers was then immersed in concentrated sulphuric acid (H_2SO_4) in order to dissolve a certain amount of fiber surface (Figure 1B). After a designated period of residence time in the acid (5−300 s) the specimens were immersed in distilled water for 10 s (Figure 1C) to partially coagulate the fibers and to prevent dissolved fiber surfaces from adhering to the glass plate, which was used for consolidation. Subsequently, mild pressure (6 kPa) was applied onto the specimens for 5 min (Figure 1D). After consolidation, the specimen was immersed in distilled water for 15 min for final coagulation (Figure 1E). Residual H_2SO_4 was extracted in a 20 wt % sodium hydroxide (NaOH) solution (Figure 1F), followed by solidification and neutralization in distilled water. The samples thus produced were kept overnight (∼18 h) in water (pH 7) for complete neutralization. Finally, the resulting specimens were dried in a vacuum oven at 80 °C for 24 h while applying a low pressure (∼1 kPa) to prevent warping. The lateral width of the composite ranged from 2.80 mm (10 s) to 1.80 mm (300 s) because of the structural contraction occurring in the process, especially during the coagulation and drying steps.

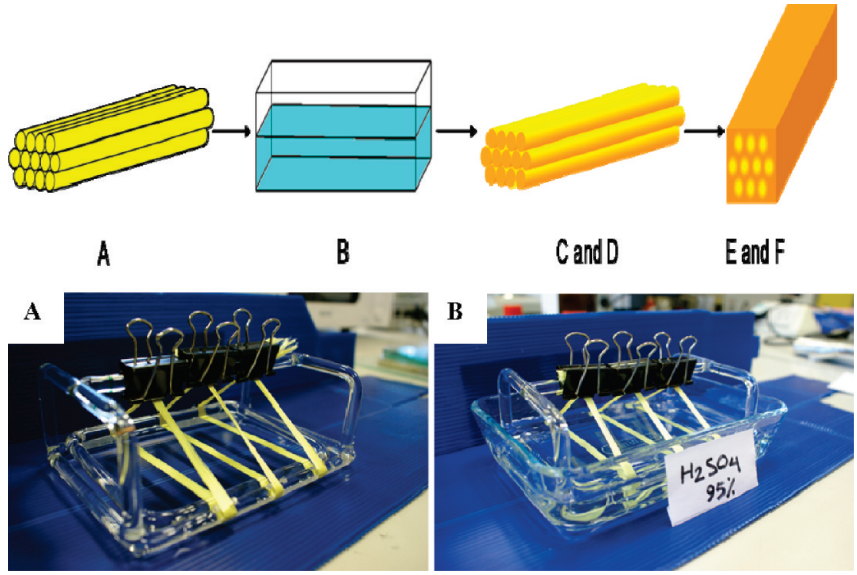

FIGURE 1. Schematics and pictures of the selective surface dissolution process of aramid fibers for preparation of "all-aramid" composite: (A) fiber alignment and constraining; (B) immersion in acid; (C) initial coagulation in water; (D) consolidation by pressure; (E) final coagulation; and (F) acid extraction.

Characterization. Tensile testing of single aramid fibers was performed on a Hounsfield tensile tester at room temperature. Specimens were prepared by mounting a single fiber onto a cardboard paper frame with a series of gauge lengths (25, 50, 100 mm). A strain rate of 0.1 min^{-1} was used and load was recorded using a 5 N load cell. For statistics, 30 single fibers were tested, and average values of tensile strength, Young's modulus and elongation at break were calculated. Mechanical properties of multi-filament yarn (1000 filaments) were measured as well, using an Instron 5566 tensile testing machine equipped with a pair of manual wedge-action grips. A fiber bundle with zero twist was mounted on a similar cardboard frame as used for the single fiber tests with a gauge length of 250 mm. A strain rate of 0.1 min^{-1} was used in the tests and at least five fiber bundles were tested.

Mechanical properties of all-aramid composites were investigated using the Instron 5566 tensile testing machine equipped with a 5 kN load cell. Tensile tests were carried out on unidirectional composites in both the longitudinal and transverse direction. Initial compliance correction was performed to eliminate the effect of system compliance due to the relatively small size of the specimens prepared. The gauge length was 15 mm for longitudinal samples and 3 mm for transverse samples. The ends of all the samples were adhesively bonded to cardboard end-tabs to assist gripping. A strain rate of 0.1 min^{-1} was used for longitudinal specimens, while a strain rate of 1 min^{-1} was employed for the transverse tests. At least five specimens of each sample produced were tested.

Dynamic mechanical analysis was performed on all-aramid composites in the orientation direction of fibers to study their thermo-mechanical properties using a TA Instrument Q800 DMA. To eliminate residual stresses, we applied a preload of 0.1 N. Specimens with a gauge length of 20 mm were subjected to sinusoidal tensile displacement with a controlled strain of 0.25 % at a frequency of 1 Hz and temperature ramped from 5 °C to 400 °C at a rate of 3 °C min^{-1}.

Scanning electron microscopy was employed using a FEI inspector-F to determine filament diameters and to investigate the (cross-sectional) morphology of all-aramid composites. Specimens were coated with carbon and the backscattering image mode was used. Wide-angle X-ray diffraction was performed on fibers as well as composites. Cu−Kα radiation, generated with an X'Pert Pro diffractometer (PANalytical) operated at 45 kV, 40 mA, was irradiated, then the diffraction profile was detected using an X-ray goniometer with symmetric reflection geometry and was resolved into noncrystalline scattering and crystalline reflections using Rigaku multipeak separation software.

RESULTS AND DISCUSSION

In an initial set of experiments, the influence of the concentration, or strength of sulphuric acid on the dissolution or swelling of PPTA filaments was investigated. Figure 2 shows the surface morphology of aramid fibers as revealed by scanning electron microscopy after immersion for 10 s in sulphuric acid of different weight concentrations (75, 85, and 95%), followed by coagulation in water.

Not surprisingly, the diameter of the acid-treated aramid fibers decreased in comparison with that of the original filaments. Furthermore, the surface topology of fibers treated with acids of different concentrations clearly varied significantly (Figure 2), indicating that different acid strengths have a different abilities of dissolving the fibers, and thus forming composites. The surface of aramid fibers immersed in 75 and 85% sulphuric acid was covered with randomly distributed swollen humps or holes. Clearly, sulphuric acid of 75 and 85% was not able to uniformly swell or dissolve the outer skin of the fibers, necessarily to bond adjacent fibers together and to form a high quality composite. On the other hand, surfaces of aramid fibers treated with 95% sulphuric acid were smooth and uniform. Therefore, 95% acid was selected as the solvent of choice for preparing all-aramid composites in this study.

For reference purposes, we revaluated values of the Young's modulus, tensile strength, and strain at break for Twaron 1000 single fiber and multi-filament yarn, which are listed in Table 1.

Single-species, all-aramid composites were prepared from aligned PPTA fibers, which were immersed in 95% H_2SO_4 for, respectively, 5, 10, 30, 60, 120, and 300 s to selectively

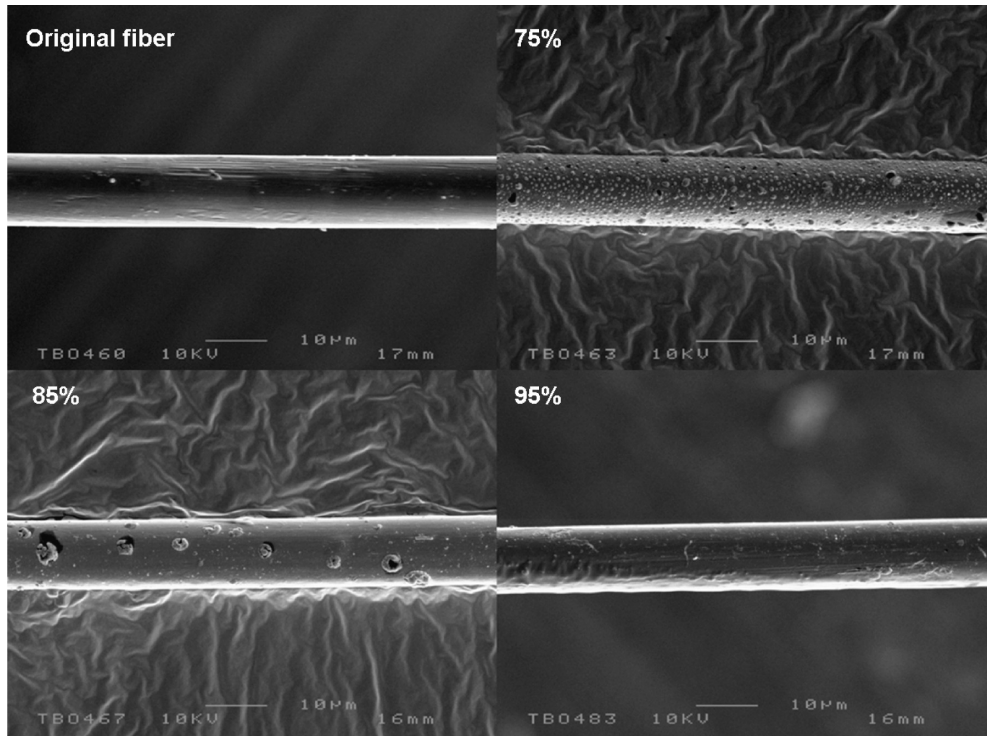

FIGURE 2. Effect of acid concentration on dissolution of single aramid fiber: original fiber; 10 s in 75%, 85%, and 95% H_2SO_4 solution, showing that 95% gives the most uniform dissolution or swelling effect. (The wrinkled background in the 75 and 85% pictures is the conducting carbon tape used to hold the fiber for SEM.)

Table 1. Mechanical Properties of Original Twaron 1000 Single Fiber and Multifilament Yarn before Surface Dissolution (Standard Deviation in Parentheses)

property	single fiber	yarn
diameter (μm)	12.3 (0.9)	
Young's modulus (GPa)	91.1[a]	54.4 (5.6)
tensile strength (GPa)	3.10 (0.26)	2.44 (0.40)[c]
strain at break (%)	3.08[a]	[b]

[a] The true fiber modulus (or strain at break) was evaluated through zero-extrapolation of the measured modulus (or strain) as a function of the inverse of the gauge length (41). [b] Multifilament yarns fail a progressive way and therefore strain at break is not reported. [c] A bundle of fibers whose single fiber elements do not possess a uniform strength is not simply the average strength of the individual fibers (42, 43). Depending on the scatter in single fiber strength, the mean yarn strength will therefore be lower than single fiber strength. For example, for a 10% variance, the mean yarn strength is expected to be about 80% that of the mean single fiber strength. Table 1 shows indeed a reduction in tensile strength and Young's modulus of the multifilament yarn compared with a single fiber.

dissolve fiber surfaces and, subsequently, consolidate them into unidirectional all-aramid composites. The thickness of the resulting composites ranged from 0.28 mm (10 s) to 0.67 mm (300 s). Figure 3 reveals that the modulus and tensile strength decreased rapidly, even for short immersion times. For instance, the modulus decreased by 33% and tensile strength by 60% for composites after immersion for only 60 s in 95% H_2SO_4. This observation is readily understood when considering that the more oriented skin region in Twaron 1000 fiber (44−46) is very thin (~150 nm) (44); this outer region rapidly dissolved followed by solvent penetrating into the less oriented internal region. After immersion for 60 s, the reduction in mechanical properties slowed down, as now only the less-oriented material in the core started to dissolve.

Conversely, but highly beneficially, the progressive formation of matrix and interphase aids to stress transfer between the filaments, as indicated by the increase in transverse properties of the composites. The transverse properties, however, are still fairly low (in MPa rather than GPa as in the case of longitudinal properties) because of the highly anisotropic nature of the PPTA fibers and possibly fiber/matrix interphase, leading to extensive fibrillation at the interphase (see also Figure 3). Figure 3 also reveals that all-aramid composites prepared with filaments immersed for 120 s in H_2SO_4 featured a good compromise between longitudinal mechanical properties and interfacial adhesion between fibers, as reflected by the transverse composite properties; the latter was corroborated by investigations of the morphology of all-aramid composites, which will be discussed below.

Figure 4a shows different failure modes of these composites for short, moderate and long immersion times of the constituent filaments. Failure-mode observations revealed the existence of a large number of non-dissolved fibers inside composites produced with filaments of short immersion time. The insufficient amount of matrix formed in these materials lead to a "brushlike" failure mode with extensive debonding. However, composites prepared with fibers immersed for 120 s in 95% sulphuric acid showed improved and more uniform adhesion. Composites produced with

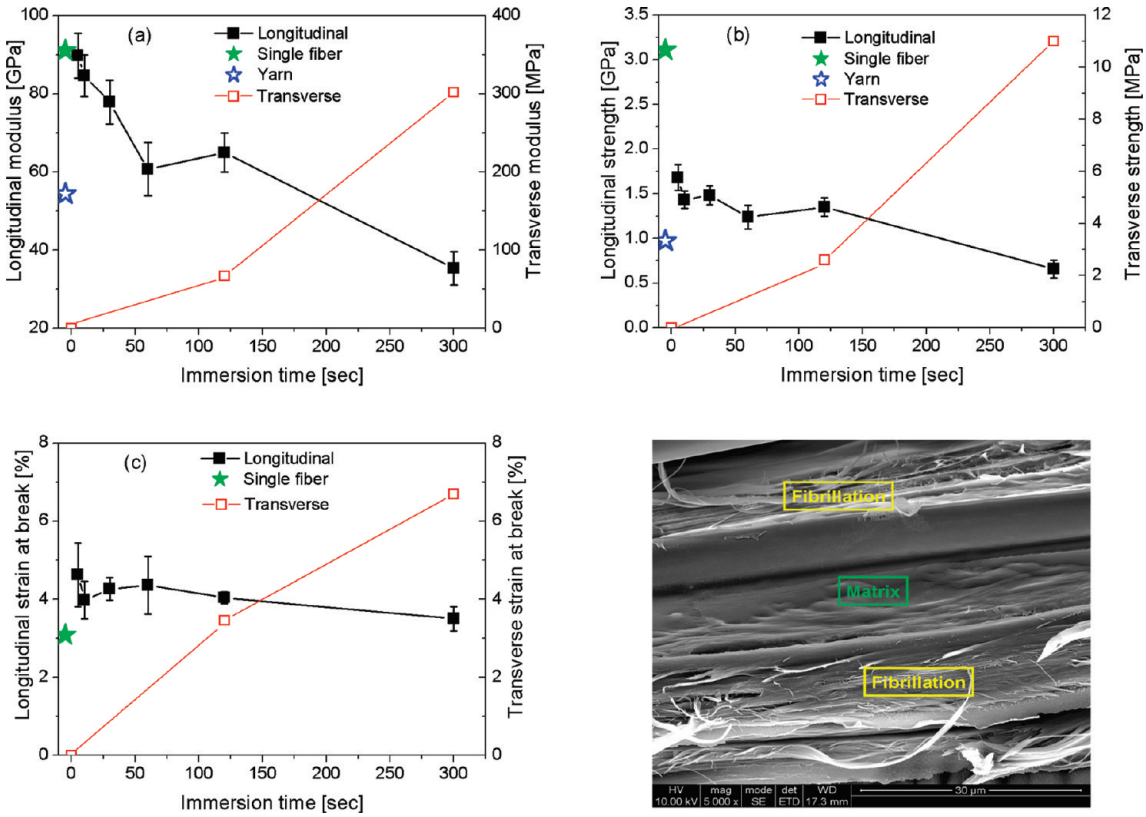

FIGURE 3. Effect of immersion time on mechanical properties of unidirectional all-aramid composites in longitudinal and transverse directions: (a) Young's modulus, (b) tensile strength, (c) strain at break; and a scanning electron micrograph of transverse failure mode, showing extensive amount of fibrillation occurred in the fiber/matrix interphase due to highly ordered fibrillar structure of aramid fiber.

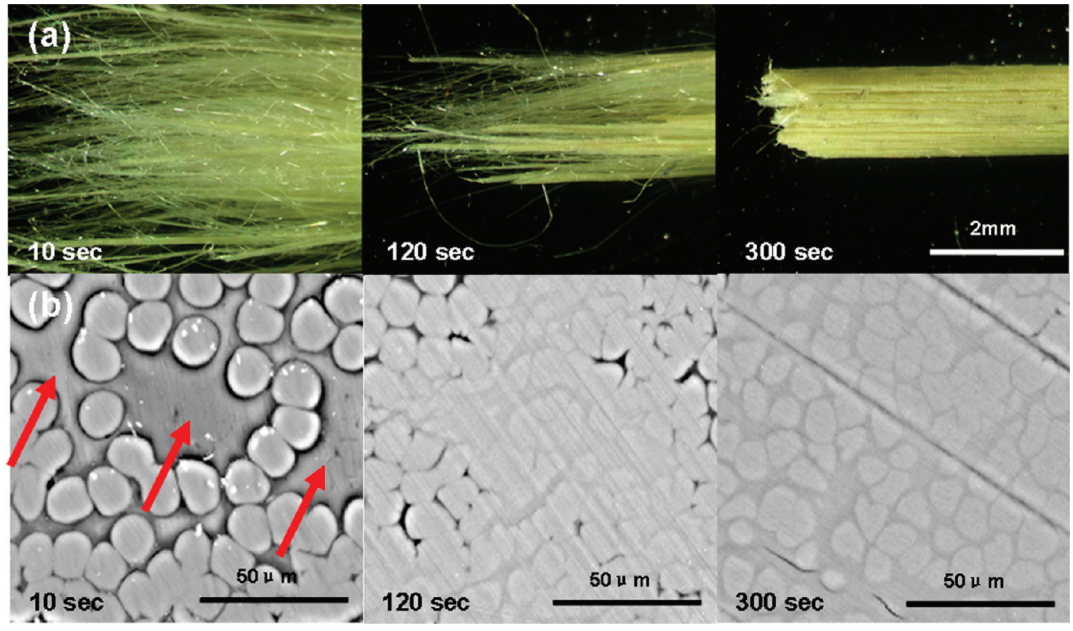

FIGURE 4. (a) Failure modes after longitudinal tensile tests of composites prepared with filaments immersed in 95% H_2SO_4 for 10 (short), 120 (medium), and 300 (long) s; (b) scanning electron micrographs of polished cross-sections of all-aramid composites prepared with filaments immersed in 95% H_2SO_4 for 10, 120, and 300 s. Areas indicated by red arrows are composed of resin employed to embed the sample for SEM preparation and represent voids inside the composite structure. A clear decrease in the number and size of voids inside the structure was observed with increasing immersion time.

filaments of 300 s immersion time appeared to be brittle, indicating very strong interfacial adhesion as large fractions of the fibers were dissolved and transformed into matrix material. The slight reduction in strain at break with increasing filament immersion time (see Figure 3), hence, is the logical result of a reduction in fiber properties in combination

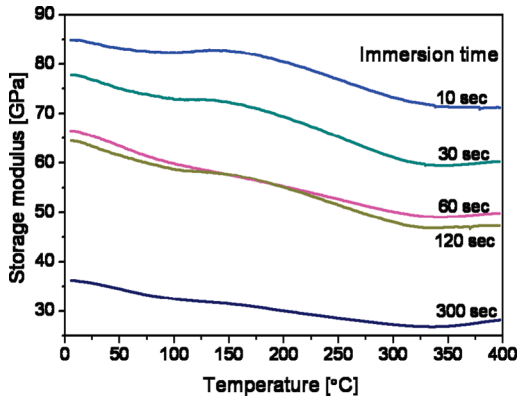

FIGURE 5. Storage modulus vs. temperature of all-aramid composites prepared with filaments immersed for different times in 95% H_2SO_4. Clearly, high modulus is retained at high temperatures. The increase in storage modulus above 350 °C is due to shrinkage of the specimens at these high temperatures.

with strong interfacial adhesion, leading to fiber−fiber interactions and a more brittle failure mode (47−51).

More detailed morphological changes in cross-sections are shown in Figure 4b. Upon longer exposure to sulphuric acid, more of the fiber skin dissolved and improved wetting of the filaments by PPTA matrix occurred, resulting in better interfacial bonding. As mentioned previously, composites prepared with filaments immersed for 120 s in 95% H_2SO_4 exhibited a good compromise between longitudinal mechanical properties and interfacial adhesion. According to morphological investigations, the outer part of dissolved fibers formed a continuous matrix after 120 s immersion time, which was adequate to bond remaining fiber cores together. This resulted in a sufficient level of adhesion between fibers while leaving a suitable fraction of the fiber cores as the reinforcing elements.

Dynamic mechanical thermal analysis (DMTA) was used to determine the temperature dependence of the composites' stiffness. In Figure 5, as expected for polymeric materials, a decrease in storage modulus with increasing temperature was observed also for the all-aramid composites. However, even at temperatures as high as 250 °C, the present composites retained a high modulus (~50 GPa; 120 s immersion time), highlighting the excellent thermal stability of these materials and their potential for high-temperature applications. Generally, the thermal stability of aramid fiber reinforced plastic is limited by the thermal stability of the polymer matrix. The most popular matrix systems for aramid fibers have been epoxy-based. These composite systems have service temperatures of around 100−120°C on a continuous basis and around 130−140°C for short duration. However, in the case of all-aramid composites, fiber, matrix, and interphase all exhibit the same high thermal stability, leading to an engineering material with excellent mechanical properties at temperatures around 250−300°C, properties that are normally attainable only with polyimide-type specialty resins.

The apparent crystallinity and crystal size of all-aramid composites was investigated by wide-angle X-ray diffraction (XRD). The original Twaron 1000 filaments show in Figure

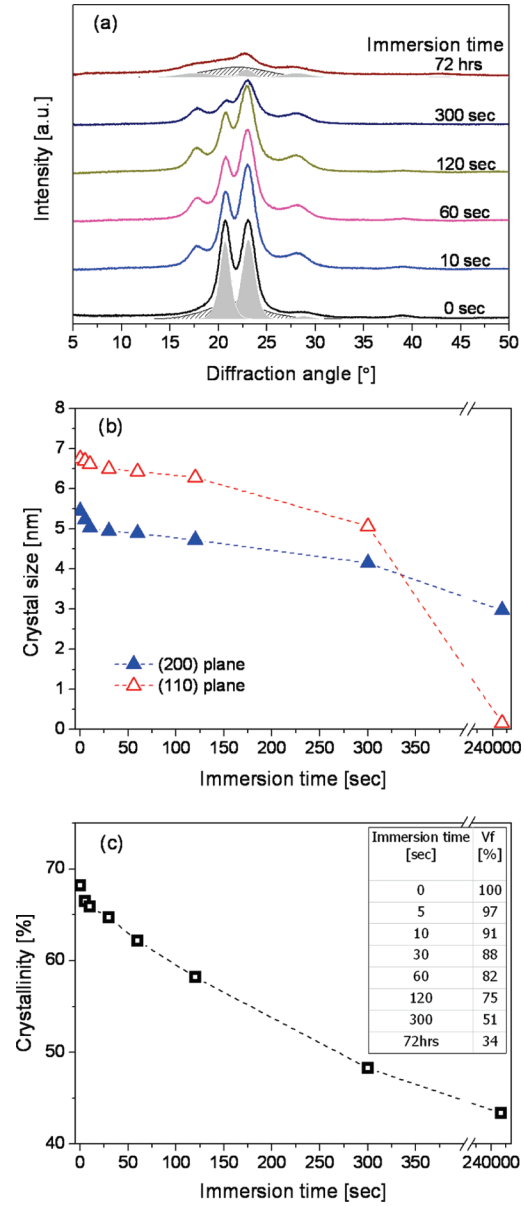

FIGURE 6. (a) Equatorial X-ray diffraction profiles of untreated fibers, and composites prepared with filaments immersed for 10, 60, 120, and 300 s in 95% H_2SO_4, and dissolved (72 h) and coagulated fibers. The grey area shows the crystalline reflections, the hatched area corresponds to the non-crystalline scattering. The apparent crystallinity was evaluated from their area ratio; (b) the effect of immersion time on crystal size of all-aramid composites; (c) effect of immersion time of PPTA filaments in 95% H_2SO_4 on the apparent crystallinity of all-aramid composites. The inset table lists the residual oriented fiber phase or "fiber volume fraction" (V_f) in the composites and was estimated from the degree of intensity reduction of the (110), (200), and (211) reflections in Figure 6a.

6a the two characteristic sharp diffraction peaks at diffraction angles (2θ) of 20.7° for the (110) plane and at 23° for the (200) plane (26, 52). XRD data also featured an increased intensity of a reflection at diffraction angle (2θ) of 17.5°, which is indicative of the modification II of PPTA. This crystal polymorph was proposed by Haraguchi and co-workers (53) for aramid film which was coagulated in water. The very strong (110) reflection in crystal modification I of aramid fiber was absent in modification II (53), which is in agreement with the decrease in the peak intensity of the (110)

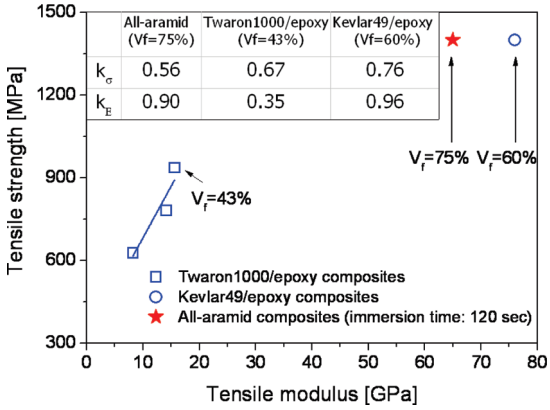

FIGURE 7. Comparison of mechanical properties of all-aramid composites prepared in this work and traditional unidirectional aramid/epoxy composites (54, 55).

plane in Figure 6a. The Bragg spacing of the (200) reflection increased in modification II because of the interaction of water molecules with hydrogen bonds (53), which explains the slight decrease in diffraction angle in Figure 6a. Clearly, with increasing immersion times, larger fractions of the fibers are dissolved to form noncrystalline or partially crystalline (e.g., modification II) matrix phase, resulting in a reduction of the overall apparent crystallinity of the final composites, which is in a good agreement with the reduction of Young's modulus in Figure 3a.

Analysis of the X-ray diffraction data was conducted by means of Scherrer's equation

$$D = \lambda/\beta\cos\theta \qquad (1)$$

Here, λ = 1.5418 Å, β represents the corrected integral width, and θ is the Bragg angle for the (110)/(200) reflection. Figure 6b shows that the crystallite size for the (110) plane decreased sharply to almost zero after a long period of filament immersion (72 h). However, the crystallite size associated with the (200) plane exhibited only a mild reduction, and remained 3 nm after 72 h treatment. These results indicate the diminishment of crystal modification I and the formation of crystal modification II in the microstructure of the all-aramid composites. Encouragingly, according to Figure 6c, all-aramid composites exhibited a higher "fiber volume fraction" than traditional aramid/epoxy composites. Even at an extremely long immersion time of 72 h, a crystallinity of 43% and residual oriented fiber phase of 34% still remained in the composites.

Figure 7 illustrates the excellent mechanical performance of the all-aramid composites compared to standard unidirectional Twaron 1000/epoxy composites (54). For comparison, the mechanical characteristics of a unidirectional aramid/epoxy composite based on the higher-modulus Kevlar 49 fiber are also plotted (55). When contrasted with such traditional aramid/epoxy composites, the present all-aramid composites have a high original reinforcement contents up to ~80 vol %. Evidently, this high reinforcement content contributes to excellent mechanical properties of the composites and compensates to some extend for the loss in properties when compared to those of single filaments and yarns through the dissolution of the highly oriented fiber skin. Compared to the impressive longitudinal properties, the transverse properties of the all-aramid composites (see Figure 3) are much lower, especially for the composites with 120 s immersion time (2.5 MPa). However, the maximum transverse tensile strength reported for an all-aramid composite with 300 s immersion time (11 MPa) is quite similar to that of a typical Kevlar 49/epoxy laminate with 60 vol % fiber at around 12 MPa (55).

For a more quantitative analysis of the mechanical properties of the present all-aramid composites, fiber efficiency factors for longitudinal tensile strength and modulus were calculated using the well-known "rule of mixture" equations (56)

$$\sigma_c = k_\sigma V_f \sigma_f + (1 - V_f)\sigma_m \qquad (2)$$

and

$$E_c = k_E V_f E_f + (1 - V_f)E_m \qquad (3)$$

where k_σ and k_E are the fiber efficiency factors for strength and modulus, respectively. σ_c and E_c are the strength and modulus of the composite, σ_f and E_f are the corresponding values of the constituting fibers, σ_m and E_m the corresponding values of the matrix, and V_f is the fiber volume fraction. To calculate k_σ and k_E for the composites in Figure 7, standard epoxy properties of σ_m = 80 MPa, E_m = 3.2 GPa were taken from a previous study (57). PPTA matrix properties of σ_m= 400 MPa, E_m = 15 GPa were taken to be those of a commercial non-oriented PPTA film, Aramica from Teijin-Asahi (58). Kevlar 49 properties of σ_f = 3000 MPa, E_f = 130 GPa was used; Twaron 1000 properties are listed in Table 1.

As the inset table in Figure 7 reveals, the efficiency factors k for all-aramid composites are reasonably high and comparable to aramid/epoxy composites. Because the rule of mixture assumes the reinforcement property in the composite similar to that measured in the single-fiber test (see Table 1), the efficiency factor k is a good indication of the relative fiber property loss due to the surface dissolution process. Only for the tensile strength is k_σ slightly less for all-aramid composites, indicating that the dissolution process led to some property reduction beyond the simple rule of mixtures predictions. This disproportional property loss in tensile strength is attributed to the dissolution of highly oriented PPTA material in the fiber skin regions.

CONCLUSIONS

In summary, a new type of "all-aramid" composite was prepared from Twaron 1000 poly(*p*-phenylene terephthalamide) (PPTA) multifilament yarns by converting partially dissolved fiber skins into a PPTA matrix phase. Based on mechanical tests and failure mode observations a preferred immersion time of 120 s in 95% sulfuric acid was found to be an optimum processing condition for the preparation of

all-aramid composites. Under these conditions, an optimum balance between longitudinal mechanical properties and interfacial adhesion was achieved. DMTA results revealed retention of a high Young's modulus for these composites up to temperatures as high as 250−300 °C, indicative of the potential of these engineering materials for high-temperature applications.

Acknowledgment. The authors thank Teijin Aramid for kindly supplying aramid fibers. Our grateful thanks are extended to Mr. John Cowley for making the specially designed glass frames; Dr. Zofia Luklinska and Mr. Mick Willis for their continuous support in SEM; Dr. Rory Wilson for his expert assistance in XRD investigations and Dr. Hanneke Boerstoel for valuable discussions.

REFERENCES AND NOTES

(1) He, T.; Porter, R. S. *J. Appl. Polym. Sci.* **1988**, *35*, 1945–1953.
(2) Teishev, A.; Incardona, S.; Migliaresi, C.; Marom, G. *J. Appl. Polym. Sci.* **1995**, *50*, 503–512.
(3) Von Lacroix, F.; Werwer, M.; Schulte, K. *Composites, Part A* **1998**, *29*, 371–376.
(4) Hine, P. J.; Ward, I. M.; Olley, R. H.; Bassett, D. C. *J. Mater. Sci.* **1993**, *28*, 316–324.
(5) Von Lacroix, F.; Lu, H. Q.; Schulte, K. *Composites, Part A* **1999**, *30*, 369–373.
(6) Yan, R. J.; Hine, P. J.; Ward, I. M.; Olley, R. H.; Bassett, D. C. *J. Mater. Sci.* **1997**, *32*, 4821–4832.
(7) Hine, P. J.; Ward, I. M.; Jordan, N. D.; Olley, R. H.; Bassett, D.C. *Polymer* **2003**, *44*, 1117–1131.
(8) Jordan, N. D.; Bassett, D. C.; Olley, R. H.; Hine, P. J.; Ward, I.M. *Polymer* **2003**, *44*, 1133–1143.
(9) Peijs, T. *Mater. Today* **2003**, *6*, 30–35.
(10) Cabrera, N.; Alcock, B.; Loos, J.; Peijs, T. *Proc. Inst. Mech. Eng., Part L* **2004**, *218*, 145–155.
(11) Alcock, B.; Cabrera, N. O.; Barkoula, N. M.; Loos, J.; Peijs, T. *Composites, Part A* **2006**, *37*, 716–726.
(12) Alcock, B.; Cabrera, N. O.; Barkoula, N. M.; Peijs, T. *Compos. Sci. Technol.* **2006**, *66*, 1724–1737.
(13) Alcock, B.; Cabrera, N. O.; Barkoula, N. M.; Spoelstra, A. B.; Loos, J.; Peijs, T. *Composites, Part A* **2007**, *38*, 147–161, 1.
(14) Alcock, B.; Cabrera, N. O.; Barkoula, N. M.; Reynolds, C. T.; Govaert, L. E.; Peijs, T. *Compos. Sci. Technol.* **2007**, *67*, 2061–2070.
(15) Alcock, B.; Cabrera, N. O.; Barkoula, N. M.; Loos, J.; Peijs, T *J. Appl. Polym. Sci.* **2007**, *104, 1*, 118–129.
(16) Alcock, B.; Cabrera, N. O.; Barkoula, N. M.; Wang, Z.; Peijs, T *Composites, Part B* **2008**, *39*, 537–547, 3.
(17) Hine, P. H.; Ward, I. M. *J. Appl. Polym. Sci.* **2003**, *91*, 2223–2233.
(18) Zhang, J. M.; Reynolds, C. T.; Peijs, T. *Composites, Part A* **2009**, *40*, 1747–1755.
(19) Pegoretti, A.; Zanolli, A.; Migliaresi, C. *Compos Sci Technol* **2006**, *66*, 1970–1979.
(20) Ward, I. M.; Hine, P. J. *Polymer* **2004**, *45*, 1413–1427.
(21) Nishino, T.; Arimoto, N. *Biomacromolecules* **2007**, *8*, 2712–2716.
(22) Qin, C.; Soykeabkaew, N.; Xiuyuan, N.; Peijs, T. *Carbohydr. Polym.* **2008**, *71*, 458–467, 3.
(23) Soykeabkaew, N.; Arimoto, N.; Nishino, T.; Peijs, T. *Compos Sci Technol* **2008**, *68*, 2201–2207.
(24) Soykeabkaew, N.; Sian, C.; Gea, S.; Nishino, T.; Peijs, T. *Cellulose* **2009**, *16*, 435–444.
(25) Soykeabkaew, N.; Nishino, T.; Peijs, T. *Composites, Part A* **2009**, *40*, 321–328.
(26) Yang, H. H. *Kevlar Aramid Fiber*; John Wiley & Sons: New York, 1993.
(27) McIntyre, J. F. Aramid Fibres. In *Solid Phase Processing of Polymers*; Ward, I. M., Coates, P. D., Dumoulin, M. M., Eds.; Hanser: Munich, 2000; pp 155−171.
(28) Smith, P.; Lemstra, P. J. *J. Mater Sci* **1980**, *15*, 505.
(29) Lemstra P. J.; Bastiaansen C. W. M.; Peijs T.; Jacobs, M. J. N. Fibres based on high-molecular weight polyethylene: Processing and applications. In *Solid Phase Processing of Polymers*; Ward, I. M., Coates, P. D., Dumoulin, M. M., Eds.; Hanser: Munich, 2000; pp 155−171.
(30) Peijs T.; Jacobs, M. J. N.; Lemstra P. J., High performance polyethylene fibers. In *Comprehensive Composite Materials*; Elsevier: Amsterdam, 2003; Chapter 1.09, pp 263−301.
(31) Northolt, M. G.; Sikkema, D. J. *Adv. Polym. Sci.* **1990**, *98*, 115.
(32) Northolt M. G.; Sikkema D. J. In *Liquid Crystal Polymers, from Structure to Applications*; Collyer, A. A., Ed.; Elsevier Applied Science: London, 1992.
(33) Kwolek, S. L. U.S. Patent 3 671 542 (1972) and U.S. Patent 3 819 587 (1974).
(34) Blades H. U.S. Patent 3 767 756 (1973) and U.S. Patent 3 869 429 (1973).
(35) Feldman, L.; Farris, R. J.; Thomas, E. L. *J. Mater. Sci.* **1985**, *20*, 2719.
(36) Hwang, C. R.; Farris, R. J.; Martin, D. C.; Thomas, E. L. *J. Mater. Sci.* **1991**, *26*, 2365–2371.
(37) Lenhert, P. G.; Adams, W. W. *Proceedings of the Materials Science and Engineering of Rigid-Rod Polymers Symposium*; Boston, Nov 28−Dec 2, 1988; Materials Research Society: Warrendale, PA, 1989; Vol. 134, p 329
(38) Martin, D.C.; Thomas, E. L. *Macromolecules* **1991**, *24*, 2450–2460.
(39) Sikkema, D. J. *Polymer* **1998**, *39*, 5981–5986, 24.
(40) Lammers, M.; Klop, E. A.; Northolt, M. G.; Sikkema, D. J. *Polymer* **1998**, *39*, 5999–6005.
(41) van den Heuvel, P. W. J.; Hogeweg, B.; Peijs, T. *Composites, Part A* **1997**, *28*, 237–249.
(42) Coleman, B. D. *J. Mech. Phys. Solids* **1958**, *7*, 60–70.
(43) Daniels, H. E. *Proc. R. Soc. London, Ser. A* **1944**, *183*, 405–435.
(44) Dobb, M. G.; Robson, R. M. *J. Mater. Sci.* **1990**, *25*, 459–464.
(45) Morgan, R. J.; Pruneda, C. O.; Steele, W. J. *J. Polym. Sci., Part B: Polym. Phys.* **1983**, *21*, 1757–1783.
(46) Panar, M.; Avakian, P.; Blume, R. C.; Gardner, K. H.; Gierke, T. D.; Yang, H. H. *J. Polym. Sci., Part B: Polym. Phys.* **1983**, *21*, 1955–1969.
(47) Madhukar, M. S.; Drzal, L. T. *J. Compos. Mater.* **1991**, *25*, 958–991.
(48) Peijs, T.; Rijsdijk, H. A.; de Kok, J. M. M.; Lemstra, P. J. *Compos. Sci. Technol.* **1994**, *52*, 449–466.
(49) van den Heuvel, P. W. J.; Peijs, T.; Young, R. J. *Compos. Sci. Technol.* **1997**, *57*, 899–911.
(50) van den Heuvel, P. W. J.; Peijs, T; Young, R. J. *J. Mater. Sci. Lett.* **1996**, *15*, 1908–1911.
(51) Venderbosch, R. W.; Peijs, T.; Meijer, H. E. H.; Lemstra, P. L. *Composites, Part A* **1996**, *27*, 895–905.
(52) Northolt, M. G. *Eur. Polym. J.* **1974**, *10*, 799–804.
(53) Haraguchi, K.; Kajiyama, T.; Takayanagi, M. *J. Appl. Polym. Sci.* **1979**, *23*, 915–926.
(54) Tarantili, P. A.; Andreopoulos, A. G. *J. Appl. Polym. Sci.* **1997**, *65*, 267–276.
(55) Tsai, S. W.; Hahn, H. T. *Introduction to Composite Materials*; Technomic Publishing: Lancaster, PA, 1980.
(56) Hull, D.; Clyne, T.W. *An Introduction to Composite Materials*, 2nd ed.; Cambridge University Press: Cambridge, U.K., 1996.
(57) Govaert, L. E.; Schellens, H. J.; Thomassen, H. J. M.; Smit, R. J. M.; Terzoli, L.; Peijs, T. *Composites, Part A* **2001**, *32*, 1697–1711.
(58) http://www.asahi-kasei.co.jp

AM900859C